

# fMRI predictors based on language models of increasing complexity recover brain left lateralization

Laurent Bonnasse-Gahot  
Centre d'Analyse et de Mathématique Sociales  
CNRS, EHESS, Paris, France  
lbg@ehess.fr

Christophe Pallier  
Cognitive Neuroimaging Unit  
CNRS, INSERM, CEA, Neurospin Center, 91191 Gif-sur-Yvette, France  
christophe@pallier.org

## Abstract

Over the past decade, studies of naturalistic language processing where participants are scanned while listening to continuous text have flourished. Using word embeddings at first, then large language models, researchers have created encoding models to analyze the brain signals. Presenting these models with the same text as the participants allows to identify brain areas where there is a significant correlation between the functional magnetic resonance imaging (fMRI) time series and the ones predicted by the models' artificial neurons. One intriguing finding from these studies is that they have revealed highly symmetric bilateral activation patterns, somewhat at odds with the well-known left lateralization of language processing. Here, we report analyses of an fMRI dataset where we manipulate the complexity of large language models, testing 28 pretrained models from 8 different families, ranging from 124M to 14.2B parameters. First, we observe that the performance of models in predicting brain responses follows a scaling law, where the fit with brain activity increases linearly with the logarithm of the number of parameters of the model (and its performance on natural language processing tasks). Second, we show that a left-right asymmetry gradually appears as model size increases, and that the difference in left-right brain correlations also follows a scaling law. Whereas the smallest models show no asymmetry, larger models fit better and better left hemispheric activations than right hemispheric ones. This finding reconciles computational analyses of brain activity using large language models with the classic observation from aphasic patients showing left hemisphere dominance for language.

## 1 Introduction

Since the seminal discovery that language disorders are most often associated with lesions to the brain's left hemisphere (Dax, 1865; Manning and Thomas-Antérion, 2011; Broca, 1865; Wernicke, 1874), the existence of a left-right asymmetry in the cortical processing of language has been amply documented through different approaches, e.g., studies of split-brain patients (Gazzaniga and Sperry, 1967), intracarotid amobarbital injections (Wada and Rasmussen, 1960), electrocortical stimulation (Penfield and Roberts, 1959), functional brain imaging (Binder et al., 1996; Just et al., 1996; Stromswold et al., 1996; Malik-Moraleda et al., 2022), and behavioral measurements such as reaction times to words presented in the left or right visual fields (Hausmann et al., 2019). All in all, even if there is clear evidence that the right hemisphere is implicated in speech and language processing (Bookheimer, 2002; Jung-Beeman, 2005; Lerner et al., 2011; Vigneau et al., 2011; Bradshaw et al., 2017), it is estimated that left hemispheric dominance for language occurs in approximately 90% of healthy individuals (Josse and Tzourio-Mazoyer, 2004; Tzourio-Mazoyer et al., 2017).

Given this state of affairs, one can only be surprised by the symmetric patterns highlighted by studies that have relied on computational models of language to predict fMRI brain time-courses in participants listening to naturalistic texts (e.g. Huth et al., 2016; Heer et al., 2017; Toneva and Wehbe, 2019; Caucheteux and King, 2022; Schrimpf et al., 2021; Pasquiou et al., 2023). For example, Huth et al. (2016) constructed word embeddings using a latent-semantic approach based on co-occurrence counts (Landauer and Dumais, 1997) and used them as predictors of brain activity while participants listened to stories. The maps revealed by this approach were strikingly symmetric. This finding was replicated in subsequent studies that have used predictors derived from more advanced language models based on LSTM (Jain and Huth, 2018) or Transformers (e.g. Toneva and Wehbe, 2019; Schrimpf et al., 2021; Pasquiou et al., 2023).

In this paper, we use neural language models of increasing size (from GPT-2 with 124 million parameters to Qwen1.5-14B with 14.2 billion parameters) to fit fMRI data obtained from participants who listened to a naturalistic text. We find that a clear left-right asymmetry emerges as the size and performance of these models increases.

## 2 Methods

### 2.1 fMRI data

***Le Petit Prince* dataset.** We use the publicly available fMRI dataset *Le Petit Prince*<sup>1</sup> which provides recordings from English, French and Chinese participants who had listened to the audiobook of *Le Petit Prince* in their native language while being scanned using functional magnetic resonance (TR=2 s; voxel size= $3.75 \times 3.75 \times 3.8$  mm). Technical details on fMRI acquisition and preprocessing can be found in the publication accompanying the dataset (Li et al., 2022). Here, we use data from 48 English speakers for whom fMRI data spatially normalized in the Montreal Neurological Institute space are available in the repository. All of them were right-handed according to the Edinburgh handedness questionnaire. For each participant, fMRI acquisition was divided into 9 runs lasting each for about 10 min.

**Additional preprocessing and creation of an average subject.** To reduce the computational burden of the study, and because we are interested in making inferences about the general population, we compute a group average from all subjects. In order to further reduce the computational cost of the study, all functional data are first resampled to 4 mm isotropic voxels, close to the original acquisition resolution. Before averaging, we compute a symmetric brain mask common to all subjects using `nilearn compute_multi_epi_mask` function with the threshold parameter set at 50%. The resulting mask, henceforth named *whole brain volume*, comprises 25877 voxels (1656 cm<sup>3</sup>). For all subjects and each run independently, voxels’ time-series are high-pass filtered with a cut-off of 128 s, linearly detrended and standardized (zero mean and unit variance). We then compute the average subject by taking the mean of all these values per voxel and per run. Finally, we trim the first 20 s and the last 20 s of each run, as these were found to present deviation artifacts, and standardize the resulting time-series.

**Inter-subjects reliable voxels.** In order to evaluate the signal-to-noise ratio in each voxel, independently of any language model, we estimate the reliability of each voxel across participants. To do so, we split the group of all 48 subjects into two equal subgroups, compute the average response for each group and predict the BOLD time series from each voxel of one group from the activity of all the voxels from the other group. The fitting procedure follows the same method described in more details below when fitting brain response with neural network activations, and is based on a linear mapping from one set of responses to another, evaluated on a held-out run through cross-validation, and regularized using ridge regression (L2). For each run, for each voxel, we thus compute the correlation between the true activity and the activity predicted from the other group of subjects, with a linear model trained on the other runs. This procedure is repeated 10 times, using different splits of the subjects.

<sup>1</sup><https://openneuro.org/datasets/ds003643/versions/2.0.1>

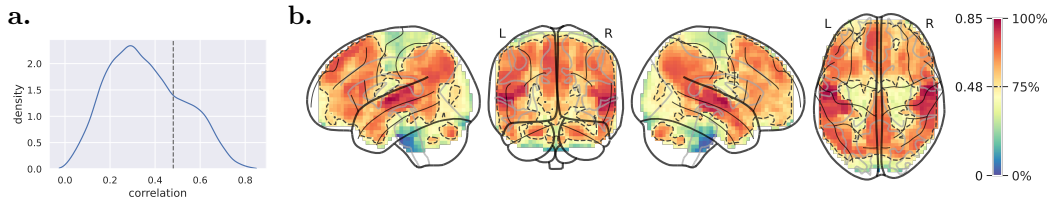


Figure 1: **Inter-subjects reliable voxels.** (a) Distribution of inter-subjects correlations over voxels, computed using two subgroups of subjects and predicting one subgroup average fMRI time-course from the other one (see main text for details). Voxels with a brain correlation above the dotted vertical line represent the 25% voxels with the largest correlations. (b) Glass brain representation of this inter-subjects reliability measure. Hot colors and dotted line show the 25% most reliable voxels.

The final inter-group correlation for each voxel is the average over these 10 trials, and is plotted in Fig. 1. The resulting map is quite consistent to the ones obtained in previous inter-subjects correlations language studies (e.g. Lerner et al., 2011). The plots presented in the paper are based on the subset of the 25% most reliable voxels, representing a total of 6469 voxels ( $414 \text{ cm}^3$ ) – 3286 in the left hemisphere and 3183 in the right hemisphere. These voxels are in hot-colored regions delineated with the dashed lines on Fig. 1. Corresponding plots computed over whole brain data are provided as supplementary figures in appendix.

**Regions of Interest.** We selected a set of a priori regions of interest from previous works on syntactic and semantic composition: the Temporal Pole (TP), anterior Superior Temporal Sulcus (aSTS) and posterior Superior Temporal Sulcus (pSTS) from Pallier et al. (2011), the Inferior Frontal Gyrus pars opercularis (BA44), triangularis (BA44) and orbitalis (BA47) from Zaccarella et al. (2017), and the Angular Gyrus/Temporal Parietal Junction (AG/TPJ) from Price et al. (2015). Each region was defined as a sphere of 10 mm radius centered on the following coordinates in the Montreal Neurological Institute’s MNI152 space : TP (-48, 15, -27), aSTS (-54, -12, -12), pSTS (-51, -39, 3), AG/TPJ (-52, -56, 22), BA44 (-50, 12, 16), BA45 (-52, 28, 10), BA47 (-44,34,-8).

## 2.2 Encoding models

**Language models.** We used 28 pretrained models, all available on the Hugging Face hub, ranging from 124M to 14.2B parameters. The full list along with some details on the number of parameters, layers and hidden size (number of neurons  $n_{\text{neurons}}$  at the output of each layer) is provided in Table A.1 on page 16 in Appendix. These pretrained models come from 8 different families, namely GPT-2 (Radford et al., 2019), OPT (Zhang et al., 2022), Llama 2 (Touvron et al., 2023), Qwen (Bai et al., 2023), gemma (Team et al., 2024), Stable LM (Bellagente et al., 2024), Mistral (Jiang et al., 2023), and Mamba (Gu and Dao, 2023). In this study, we only consider base models, trained with the same next-word prediction task. Most models are based on the Transformer decoder architecture (Vaswani et al., 2017), apart from the Mamba family, which is a recent come-back of the recurrent neural network approach that is competitive with the Transformer language models.

In order to extract the activation of each model in response to the text of *The Little Prince*, each model is fed with the full original English text. We make use of the time-aligned speech segmentation provided in the *Le Petit Prince* openneuro.org repository, to align the activity of the neural networks with what the subjects heard in the scanner. Each word in the text is associated with its onset in the audiobook, and the representation that we compute is the average of all the vectors of all the tokens that constitute this word, as well as the following punctuation marks if there are any. Finally, in order to mimic the BOLD response, the activity of the artificial neural network under consideration is convolved with the Glover haemodynamic response function (Glover, 1999), as implemented in the `nilearn` package.

**Baseline models.** In addition to considering all these pretrained language models, we look at a few baselines to compare with. First, we consider purely random vectors, aligned with the word onsets. Second, we consider random embeddings, similar to the previous case, but where each word is always associated with the same (random) vector. In these two cases, we look at 300 and 1024 dimensional vectors. The results presented in this paper for these random baselines were averaged over 10 models obtained from different seeds. Third, we look at non-contextual embeddings provided by the seminal GloVe embeddings, where each word is always associated with the same vector, of 300 dimensions here, after training on co-occurrences on large English text corpora (Pennington et al., 2014).

**Procedure for fitting an encoding model.** For each model, we separately consider the activity provided by each layer, plus the embedding layer. Hence, for a 12-layer model, we consider 13 layers. Let us notate  $X_{l,k}$  the activity of a layer  $l$  generated by the text of run  $k$ , (after convolution with the haemodynamic response function, as described above), and  $Y_{v,k}$  the BOLD time series of voxel  $v$  of run  $k$ .  $X_{l,k}$  is a  $n_{\text{scans},k} \times n_{\text{neurons}}$  matrix, and  $Y_{v,k}$  a vector of dimension  $n_{\text{scans},k}$ , where  $n_{\text{scans},k}$  is the number of scans of run  $k$ , and  $n_{\text{neurons}}$  the number of dimensions of layer  $l$  (for instance, gpt2-large model has 1280 dimensions, and Mistral-7B-v0.1 has 4096 dimensions). The goal is to predict the functional brain activity  $Y_{v,k}$  using the artificial neural activity  $X_{l,k}$  as regressors, simply using a linear mapping between the two:  $Y_{v,k} = X_{l,k}\beta$ , where  $\beta$  is a vector of dimension  $n_{\text{neurons}}$ . In order to avoid overfitting, the  $\beta$  coefficients are determined using ridge regression with regularization strength controlled by the parameter  $\alpha$ . More precisely, given a run  $k$  used as test, all the remaining 8 runs are used as training set to determine the  $\beta$  coefficients. The hyperparameter  $\alpha$  is chosen using nested cross-validation among a range of possible values (16 values log-spaced between  $10^2$  and  $10^7$ ): among the runs used for training, one is used for validation, and the remaining 7 runs for training the ridge regression with each value of  $\alpha$ . Correlation between the actual values  $Y_{v,\text{val}}$  and the predicted ones  $\widehat{Y_{v,\text{val}}}$  is used to decide which value of  $\alpha$  is used during training: the best  $\alpha$  is chosen as the one yielding the greatest correlation averaged over all voxels<sup>2</sup>. This value is then used to compute the ridge regression on the training runs and predict the functional brain activity on the test run  $k$ . The brain correlation for a given voxel  $v$  and a given layer  $l$  is given by repeating this procedure for all 9 runs and taking the average correlation:  $1/n_{\text{runs}} \sum_{k=1}^{n_{\text{runs}}} \text{corr}(Y_{v,k}; \widehat{Y_{v,k}})$ . In the end, for a given voxel, we take as brain correlation the best correlation when considering all the layers of the model.

## 2.3 Computer code

The Python 3.10 code written for the present project relies on the following libraries: `transformers` v4.40.1 (Wolf et al., 2020), `scikit_learn` v1.4.2 (Pedregosa et al., 2011), `nilearn` v0.10.4, `Pytorch` v2.3.0 (Paszke et al., 2019), `matplotlib` v3.8.4 (Hunter, 2007), `seaborn` v0.13.2 (Waskom, 2021), `numpy` v1.26.4 (Van Der Walt et al., 2011), `pandas` v2.2.2 (McKinney et al., 2010), `statsmodels` v0.14.2 (Seabold and Perktold, 2010). All pretrained models were downloaded from Hugging Face through the `transformers` interface. The code is available at [https://github.com/1-bg/1lms\\_brain\\_lateralization](https://github.com/1-bg/1lms_brain_lateralization).

The whole study took about 5 five days of CPU time on a computer equipped with an Intel Xeon w5-3425 processor (12 cores), mainly dedicated to perform the ridge regression of all layers of all models, using the `scikit-learn` package.

# 3 Results

## 3.1 Distribution of correlations

The distributions of correlations over voxels, for each model, are displayed on panel (a) of Fig. 2 for the 25% most reliable voxels, and of Fig. B.1 for the whole brain volume.

<sup>2</sup>We performed exploratory analyses showing that a single value for  $\alpha$  for all the voxels in the brain was not detrimental to the predictions of the functional data, and produced a massive gain in speed.

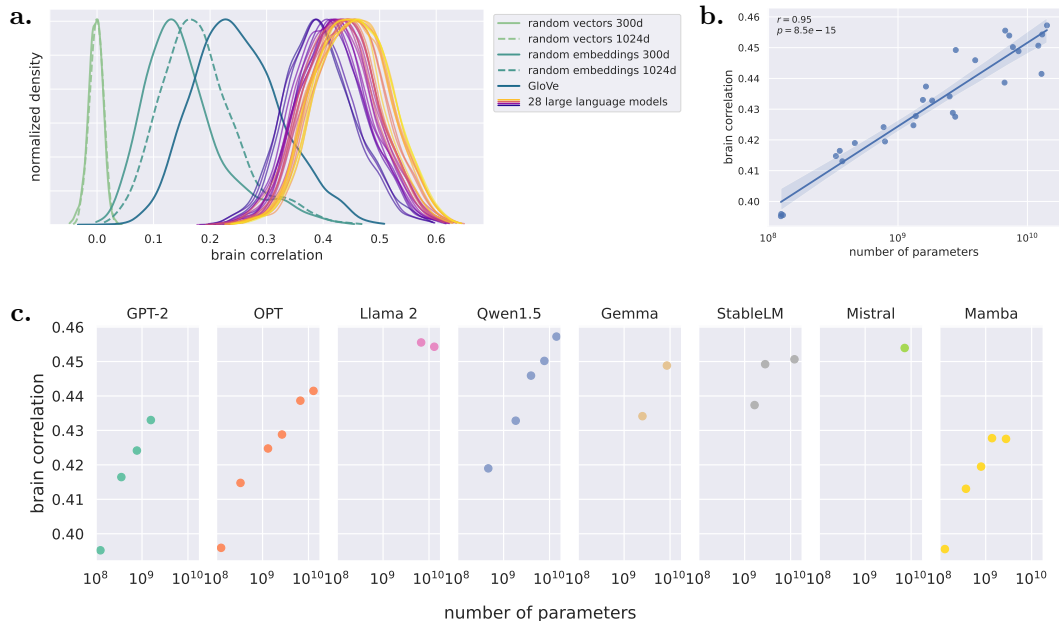


Figure 2: **Performance of various models in predicting fMRI brain time-courses.** (a) Density estimates of the distributions of  $r$ -scores obtained for all 28 large language models, the random baselines and GloVe. The densities are scaled to have the same maximum (b) Average  $r$ -score as a function of the logarithm of model’s size. Here and in the next figures, the shaded area indicates the 95% confidence interval of the slope, computed with bootstrap. (c) Same, split by models’ family.

The random vector baseline yields very low brain correlations centered around 0. Random embeddings (fixed random vector for each word) show positive correlations, especially in the 25% most reliable voxels mask, and it increases with the dimension of the embeddings from 300 to 1024. GloVe word embeddings perform better than these baselines. Finally, the contextual embeddings provided by the large language models yield even higher brain correlations.

### 3.2 Scaling law of fMRI encoding models

Focusing on the contextual large language models, panel (b) of Fig. 2 shows the relationship between the size of the language models and their prediction performance, that is, the average correlation across the 25% most reliable voxels. The linear correlation between the brain correlation and the logarithm of the number of parameters is  $r = 0.95, p = 8.5e - 15$ . The corresponding plot for the whole volume, displayed in panel (b) of Fig. B.1, also shows a linear relationship ( $r = 0.95, p = 3.1e - 14$ ). This finding replicates the scaling law first described by Antonello et al. (2024).

The panel (c) of Fig. 2 details the results by the family of models. Within each family (except Llama 2), the scaling law roughly holds. Older models like the ones from the OPT family perform worse than more recent ones like Mistral or Qwen, although within the same family the scaling law holds well in general, as exemplified by the GPT-2, OPT or Qwen1.5 families. Interestingly, the Mamba family, which is based on a recurrent neural network architecture, contrary to all the other models which are based on the Transformer decoder, has similar performances as encoding models of brain functional data, although it lies at the bottom of the envelope of the results (see Fig. B.2). In addition, we performed an analysis of the fit as a function of layer depth, depicted in Fig. B.3. The results confirms earlier reports by Toneva and Wehbe (2019) and Caucheteux and King (2022) that the middle layers are the most predictive ones.

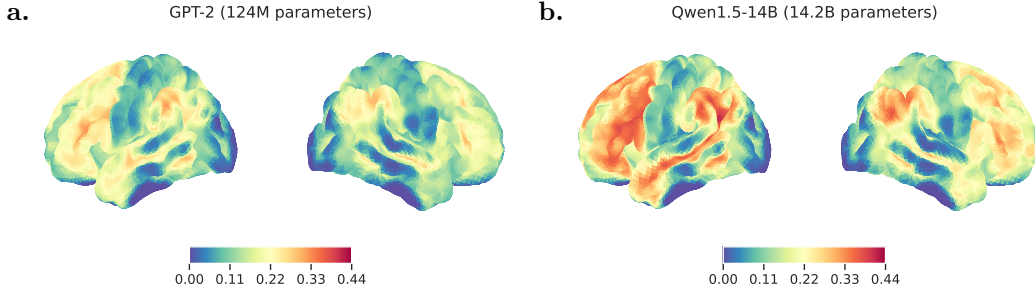


Figure 3: **Brain correlation maps associated to the smallest (a) and the largest model (b).** These maps show the increase in  $r$ -score relative the model using the random embedding baseline 1024d.

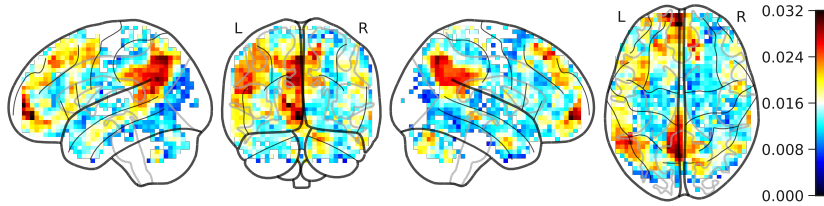


Figure 4: **Voxel-wise strength of the relationship between models’ size and their predictive power.** The slopes of the linear regression between  $r$ -score and the logarithm of the number of parameters are presented on a glass brain view. For readability, only voxels with  $p$ -values smaller than  $10^{-7}$  are shown.

**Brain maps of smallest vs. largest models.** Fig. 3 shows the brain correlations maps associated to the two most extreme models: GPT-2 with the smallest number of parameters and Qwen1.5-14B with the largest number of parameters. Interestingly, while the map generated by GPT-2 is quite symmetric, Qwen1.5-14B fits fMRI responses better in the left hemisphere than in the right (while overall performing better than GPT-2).

**Voxel-wise sensitivity to model size.** To investigate the strength of the relationship between model size and brain score in each voxel, we compute the slope of the linear regression line between the logarithm of the number of parameters and the correlation score. These slopes are displayed in Fig. 4. The strongest effects of model size are detected in the left angular gyrus, the medial prefrontal cortex and the precuneus on the medial surface of the parietal lobe. Smaller effects are detected in the middle temporal and inferior frontal gyri.

**Brain correlation and performance on natural language tasks.** The number of parameters of a model is a rough proxy of its performance on language tasks. For example, OPT-13B is found to have lower performances on various natural language processing tasks than Mistral-7B which has almost half the number of parameters. Hence, we also looked at measures of models’ performances beyond their raw number of parameters. First we compute the perplexity of all the models on the Wikitext-2 test set (Merity et al., 2016). Second we look at the Hellaswag benchmark (Zellers et al., 2019) which aims to measure the ability of a model to understand language. This measure was found to be quite challenging for language models, and the performance of models scale on this benchmark well with the training budget, either in terms of number of parameters or number of tokens seen during training (see Touvron et al., 2023). Fig. 5 shows how brain correlation increases with better models, either as measured by lower perplexity on the Wikitext-2 test set or on the Hellaswag benchmark. Both measures exhibit strong correlation with brain fit ( $r = -0.91, p = 9.5e - 12$  for perplexity and  $r = 0.95, p = 5.2e - 15$  for Hellaswag). But this is particularly relevant when looking at the ten largest models, with number of parameters above 3 billions: whereas the correlation between brain score and number of parameters is no longer significant in this case ( $r = 0.28, p = 0.4$ ), the other measures of performance display a significant correlation

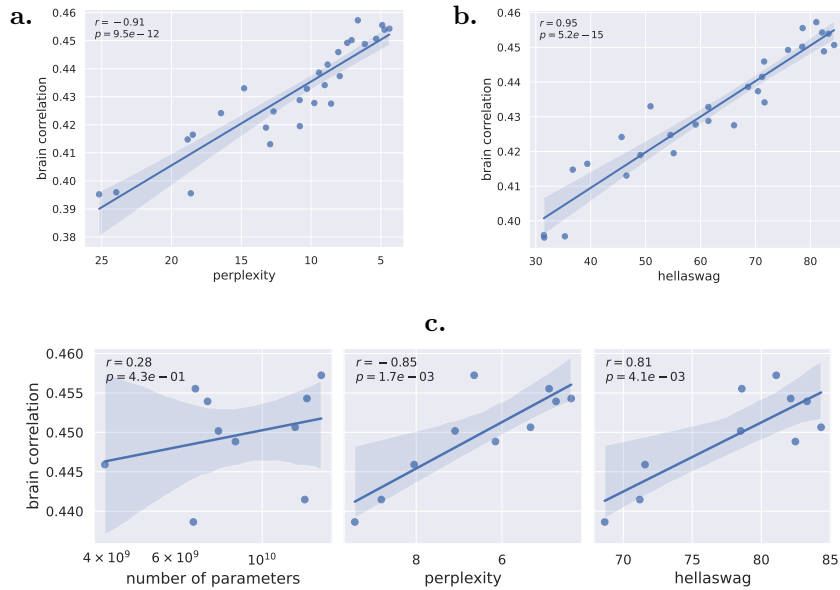


Figure 5: **Brain correlation and performance on natural language tasks.** (a) Brain correlation on the 25% most reliable voxels for all 28 large language models as a function of perplexity on Wikitext-2 test set. Note that the x-axis is inverted, as the lower the perplexity the better the model. (b) Same with performance on the Hellaswag benchmark. The higher the better. (c) Same as Fig. 2b and (a) and (b), but focusing on the 10 largest models, with a number of parameters above 3B. See Fig. B.4 for similar plots on the whole brain volume.

( $r = -0.85, p = 1.7e - 3$  for perplexity and  $r = 0.81, p = 4.1e - 3$  for Hellaswag): see Fig. 5.

### 3.3 Left-right hemispheric asymmetry

**Voxel-based analyses.** The maps presented on Fig. 3 and Fig. 4 hint at left-right differences. Therefore, we plot the relationships between model size and brain scores split by hemisphere in panel (a) of Fig. 6. This graphics reveals that the larger the model, the stronger the left-right asymmetry. More precisely, while the smallest models have similar  $r$ -scores both in the left and right hemisphere, the largest models yield stronger  $r$ -scores in the left one. The interaction between model size and hemisphere can be assessed by the correlation between model size and the left-right difference in  $r$ -scores, displayed in panel (b) of Fig. 6; its  $p$ -value is  $2.8e^{-10}$ . This graphics shows that the difference also follows a scaling law. See Fig. B.5 for the same analysis on the whole brain volume.

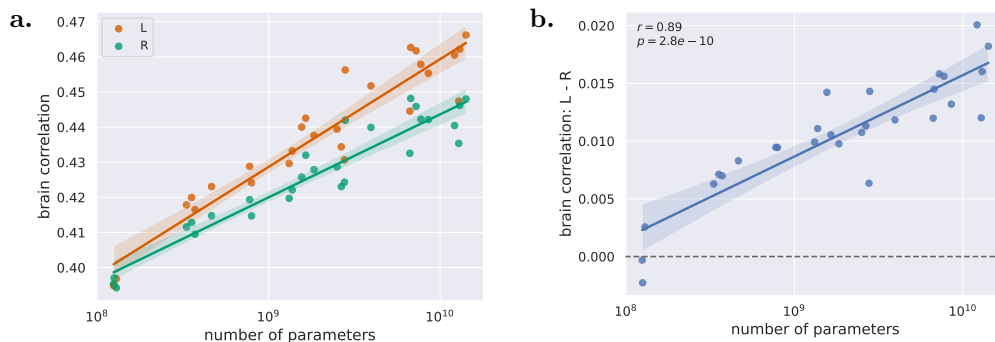


Figure 6: **Emergence of left lateralization with the size of the encoding models.** (a) Brain correlations on the 25% most reliable voxels as a function of the number of parameters, for the left hemisphere (red) and for the right hemisphere (green). (b) The difference between left and right hemispheric brain correlations also shows a scaling law.

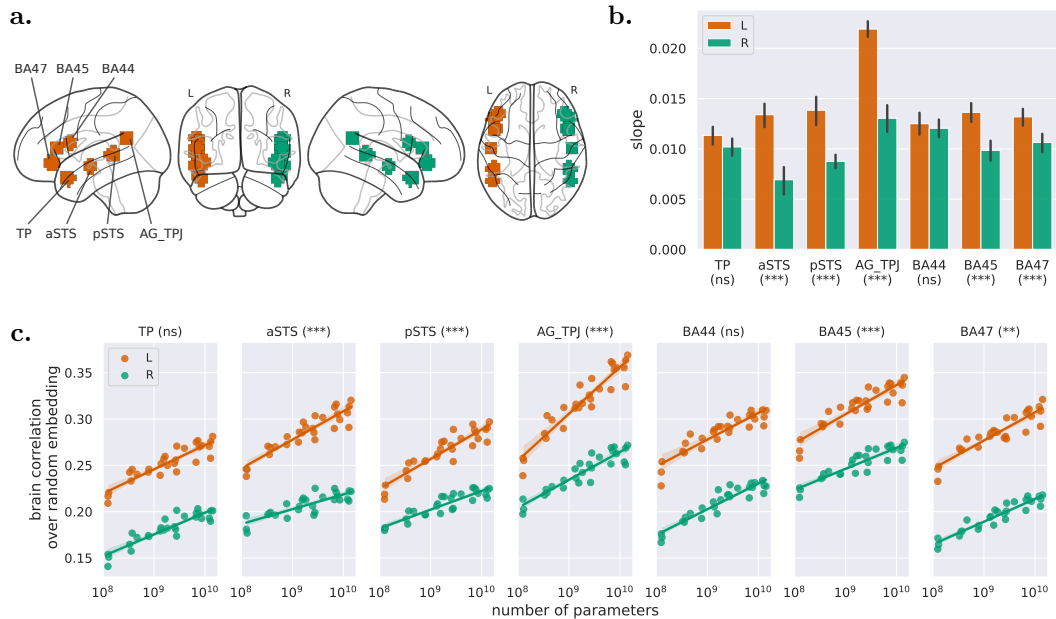


Figure 7: **Model size impact in various Regions of Interest.** (a) Locations of ROIs. (b) Slope in  $r$ -score as a function of the logarithm of the number of parameters, averaged over all voxels of a given ROI. Error bars indicate 95% confidence interval, estimated by bootstrap. The annotation below each ROI label indicates an estimate of the level of statistical significance of the difference between the slopes of the voxels of a left ROI compared to its respective right ROI (ns: non significant, \*:  $p < 0.05$ , \*\*:  $p < 0.01$ , \*\*\*:  $p < 0.001$ ). (c) Brain correlations over the random embedding baseline (see Fig. B.6 on page 20 for similar plots with raw brain correlations), as a function of the logarithm of the number of parameters. The annotation next to each ROI label indicates the level of statistical significance of the correlation between the difference in  $r$ -scores of the models on the left hemisphere minus the right hemisphere, as a function of the logarithm of the number of parameters, testing the interaction between hemisphere and model size. See Table A.2 for full statistics.

**Analyses in Regions of Interest.** The relationships between model size and  $r$ -scores in seven regions of interest from the language network in the left hemisphere, and in their mirror-image regions in the right hemisphere, are plot on Fig. 7. Brain scores improves with model size in all regions, both in the left and in the right hemisphere. Except for pars opercularis (BA44) in the inferior frontal gyrus, and for the temporal pole (TP), a left-right asymmetry in favor of the left emerges when model size increases. The steepest effect occurs in the Angular gyrus/Temporo-parietal. This region, AG\_TPJ, was already highlighted in Fig. 4 showing the slopes in individual voxels.

## 4 Discussion & Conclusion

By manipulating the size of artificial neural language models used to fit fMRI data of naturalistic language comprehension, we observed:

1. a linear relationship between the  $r$ -score (the cross-validated correlation between fMRI signal and the models' predicted time-courses), and model size (the logarithm of number of parameters): see Fig. 2.
2. a breaking down of this relationship when focusing on the most complex models – with more than 3 billions parameters. Yet, in this range, indices assessing the performance of the model on NLP tasks are still predictive of brain score (see Fig. 5).
3. a left-right asymmetry emerging when encoding models are based on increasingly complex models. The relationship between asymmetry and model size (in log number of parameters) itself follows a linear relationship (see Fig. 6).

The first observation replicates the finding of Antonello et al. (2024) who first described a scaling law between model size and brain score, extending to brain data the scaling laws observed between model size and performance on various NLP tasks (Kaplan et al., 2020). Here, we generalize their result to a different dataset and using a larger variety of models and families that notably include a non-Transformer, Mamba.

The second point, concerning the relationship between neural network models performance in NLP tasks and brain scores, was also investigated by Schrimpf et al. (2021) and by Caucheteux and King (2022). Both teams reported that brain scores generally improved as the performance in the next word prediction task increased, extending to the field of language processing results that were found in the visual domain by Schrimpf et al. (2020) or in the auditory domain by Kell et al. (2018). Caucheteux and King found that brain scores reached a plateau, and even dropped somewhat (see their Fig.2g), but we do not observe a plateau effect, which might be due to an overspecialization to the next word prediction task in their study. It should be noted that our large models are much bigger than those used in either studies, and have perplexities that are very low compared to them. It will be interesting for future work to consider even larger pretrained models to see if and when a plateau is reached.

The third point is the emergence of an asymmetry with increasing model size, an observation that has not been reported in the literature. A quick but vague explanation is that larger models better capture language representations in the left hemisphere. It begs the question of which representations are improved in larger models relative to smaller ones. For example, is it lexical, syntactic, semantic, pragmatic or world knowledge? The present work calls for detailed comparisons of the features discovered by large vs small language models, and how and where this translates into better fMRI prediction.

One can attempt to perform inverse inference, that is, try to infer which processes are involved from the brain areas highlighted by our analyses, keeping in mind the pitfalls of such an approach (Poldrack, 2011). The cortical areas where model size has the strongest impact are the Angular gyrus, the Precuneus and the medial prefrontal cortex (mPFC). These regions are also those where the effects of training a (small) network are the strongest Pasquiou et al. (2022) and were fit by models trained on semantic but not on syntax by Pasquiou et al. (2023). These regions are not specific to language, e.g. they are part of the default mode network, but are involved in the highest levels of language comprehension (Simony et al., 2016; Chang et al., 2022). The mPFC and Precuneus are known to be sensitive to discourse coherence (Ferstl and von Cramon, 2001; Xu et al., 2005). The Angular Gyrus is also considered part of the semantic system (Seghier et al., 2010; Binder and Desai, 2011; Price et al., 2015; Kuhnke et al., 2023). This suggests that the main effect of increasing model size is to improve the model capabilities at the semantic and pragmatic levels. The analysis by regions of interest revealed that the asymmetry holds in most regions of the core language network, except pars opercularis (BA44) and the Temporal Pole. The left BA44 has been associated with syntax (Zaccarella and Friederici, 2016) and/or speech processing (Matchin and Hickok, 2020). The temporal poles, both on the left and on the right, are linked to semantic processing (Pobric et al., 2010; Pyllkkänen, 2019) and have been designated as an amodal semantic hub by Patterson and Lambon Ralph (2016) (but see Snowden et al., 2018).

Despite the asymmetries observed in other regions, it is remarkable that the largest models' fits always improve over the smallest models even in the right hemisphere. It has been known for long that the right hemisphere has some language capacity (Bradshaw et al., 2017), which can manifest for example in split brain patients, or in patients with lesions in the left hemisphere. The right hemisphere is usually "hidden" because it is inhibited by the left hemisphere in healthy people (Vigneau et al., 2011). Speech prosody is usually considered to be mostly processed in the right temporal lobe (Wildgruber et al., 2006) and the right hemisphere seems to contribute to higher level aspects of language processing such as comprehending metaphors or jokes, detecting story inconsistencies (Jung-Beeman, 2005; Bookheimer, 2002).

An interesting follow-up for future work would be to see how the lateralization develops

over time during the training process of a (very) large language model, either by training such a model from scratch or by having access to checkpoints during the training (see Antonello et al., 2024; Pasquiou et al., 2022, for first attempts). In humans, it seems that language processing in the brain starts bilaterally and then becomes lateralized over time (Szaflarski et al., 2006; Olulade et al., 2020; Ozernov-Palchik et al., 2024), although some studies have found very early lateralization (Witelson and Pallie, 1973; Wood et al., 2004). Given our results on how better models recover the lateralization, we might expect the same to be true during the training process of a given model.

## Limitations

1. Our analyses were performed at the group level, on data averaged over 48 right-handed participants. Performing similar analysis on individuals might be interesting to assess inter-individual variability. However, this would require a random sample of the population, not only right-handed participants, and, more crucially, an independent assessment of hemispheric dominance of these individuals, i.e. another measures of the asymmetry. In itself, we would not expect much novel insights from such an analysis.
2. We only analyzed data from English speakers. There is no reason to expect that our result is language-specific. From the neuro-linguistic point of view, left dominance is universal (Malik-Moraleda et al., 2022), and is even attested in sign language (Poizner et al., 1987). Nevertheless, it would be nice to generalize this inquiry to other languages. As *Le Little Prince* dataset comprises fMRI data from French & Chinese speakers, one could perform similar analyses on these language. Basically, this would require more pretrained models (and compute budget).

## References

- Antonello, R., Vaidya, A., and Huth, A. (2024). Scaling laws for language encoding models in fMRI. *Advances in Neural Information Processing Systems*, 36.
- Bai, J., Bai, S., Chu, Y., Cui, Z., Dang, K., Deng, X., Fan, Y., Ge, W., Han, Y., Huang, F., et al. (2023). Qwen technical report. *arXiv preprint arXiv:2309.16609*.
- Bellagente, M., Tow, J., Mahan, D., Phung, D., Zhuravinskyi, M., Adithyan, R., Baicoianu, J., Brooks, B., Cooper, N., Datta, A., et al. (2024). Stable lm 2 1.6 b technical report. *arXiv preprint arXiv:2402.17834*.
- Binder, J. R. and Desai, R. H. (2011). The neurobiology of semantic memory. *Trends in Cognitive Sciences*, 15(11):527–536.
- Binder, J. R., Swanson, S. J., Hammeke, T. A., Morris, G. L., Mueller, W. M., Fischer, M., Benbadis, S., Frost, J. A., Rao, S. M., and Houghton, V. M. (1996). Determination of language dominance using functional MRI: a comparison with the Wada test. *Neurology*, 46(4):978–984.
- Bookheimer, S. (2002). Functional MRI of Language: New Approaches to Understanding the Cortical Organization of Semantic Processing. *Annual Review of Neuroscience*, 25(1):151–188.
- Bradshaw, A. R., Thompson, P. A., Wilson, A. C., Bishop, D. V., and Woodhead, Z. V. (2017). Measuring language lateralisation with different language tasks: a systematic review. *PeerJ*, 5:e3929.
- Broca, P. (1865). Sur le siège de la faculté du langage articulé. *Bulletins et Mémoires de la Société d’Anthropologie de Paris*, 6(1):377–393.
- Caucheteux, C. and King, J.-R. (2022). Brains and algorithms partially converge in natural language processing. *Communications biology*, 5(1):1–10.
- Chang, C. H. C., Nastase, S. A., and Hasson, U. (2022). Information flow across the cortical timescale hierarchy during narrative construction. *Proceedings of the National Academy of Sciences*, 119(51):e2209307119. Publisher: Proceedings of the National Academy of Sciences.
- Dax, M. D. (1865). Lésions de la moitié gauche de l’encéphale coïncidant avec l’oubli des signes de la pensée: Lu au Congrès méridional tenu à Montpellier en 1836, par le docteur Marc Dax. *Gazette Hebdomadaire de Médecine et de Chirurgie*, 17:259–260.
- Ferstl, E. C. and von Cramon, D. Y. (2001). The role of coherence and cohesion in text comprehension: an event-related fMRI study. *Cognitive Brain Research*, 11(3):325–340.
- Gazzaniga, M. S. and Sperry, R. W. (1967). Language after section of the cerebral commissures. *Brain*, 90(1):131–148. Publisher: Oxford University Press.
- Glover, G. H. (1999). Deconvolution of impulse response in event-related BOLD fMRI. *Neuroimage*, 9(4):416–429.
- Gu, A. and Dao, T. (2023). Mamba: Linear-time sequence modeling with selective state spaces. *arXiv preprint arXiv:2312.00752*.
- Hausmann, M., Brysbaert, M., van der Haegen, L., Lewald, J., Specht, K., Hirnstein, M., Willemin, J., Barton, J., Buchilly, D., Chmetz, F., Roch, M., Brederoo, S., Dael, N., and Mohr, C. (2019). Language lateralisation measured across linguistic and national boundaries. *Cortex*, 111:134–147.
- Heer, W. A. d., Huth, A. G., Griffiths, T. L., Gallant, J. L., and Theunissen, F. E. (2017). The Hierarchical Cortical Organization of Human Speech Processing. *Journal of Neuroscience*, 37(27):6539–6557. Publisher: Society for Neuroscience Section: Research Articles.

- Hunter, J. D. (2007). Matplotlib: A 2D graphics environment. *Computing in Science & Engineering*, 9(3):90–95.
- Huth, A. G., De Heer, W. A., Griffiths, T. L., Theunissen, F. E., and Gallant, J. L. (2016). Natural speech reveals the semantic maps that tile human cerebral cortex. *Nature*, 532(7600):453–458.
- Jain, S. and Huth, A. (2018). Incorporating context into language encoding models for fmri. *Advances in neural information processing systems*, 31.
- Jiang, A. Q., Sablayrolles, A., Mensch, A., Bamford, C., Chaplot, D. S., Casas, D. d. l., Bressand, F., Lengyel, G., Lample, G., Saulnier, L., et al. (2023). Mistral 7B. *arXiv preprint arXiv:2310.06825*.
- Josse, G. and Tzourio-Mazoyer, N. (2004). Hemispheric specialization for language. *Brain Research Reviews*, 44(1):1–12.
- Jung-Beeman, M. (2005). Bilateral brain processes for comprehending natural language. *Trends in Cognitive Sciences*, 9(11):512–518.
- Just, M. A., Carpenter, P. A., Keller, T. A., Eddy, W. F., and Thulborn, K. R. (1996). Brain activation modulated by sentence comprehension. *Science*, 274(5284):114–116.
- Kaplan, J., McCandlish, S., Henighan, T., Brown, T. B., Chess, B., Child, R., Gray, S., Radford, A., Wu, J., and Amodei, D. (2020). Scaling laws for neural language models. *arXiv preprint arXiv:2001.08361*.
- Kell, A. J., Yamins, D. L., Shook, E. N., Norman-Haignere, S. V., and McDermott, J. H. (2018). A task-optimized neural network replicates human auditory behavior, predicts brain responses, and reveals a cortical processing hierarchy. *Neuron*, 98(3):630–644.
- Kuhnke, P., Chapman, C. A., Cheung, V. K. M., Turker, S., Graessner, A., Martin, S., Williams, K. A., and Hartwigsen, G. (2023). The role of the angular gyrus in semantic cognition: a synthesis of five functional neuroimaging studies. *Brain Structure and Function*, 228(1):273–291.
- Landauer, T. K. and Dumais, S. T. (1997). A solution to Plato’s problem: The latent semantic analysis theory of acquisition, induction, and representation of knowledge. *Psychological review*, 104(2):211. Publisher: American Psychological Association.
- Lerner, Y., Honey, C. J., Silbert, L. J., and Hasson, U. (2011). Topographic Mapping of a Hierarchy of Temporal Receptive Windows Using a Narrated Story. *Journal of Neuroscience*, 31(8):2906–2915.
- Li, J., Bhattasali, S., Zhang, S., Franzluebbbers, B., Luh, W.-M., Spreng, R. N., Brennan, J. R., Yang, Y., Pallier, C., and Hale, J. (2022). Le petit prince multilingual naturalistic fmri corpus. *Scientific data*, 9(1):530.
- Malik-Moraleta, S., Ayyash, D., Gallée, J., Affourtit, J., Hoffmann, M., Mineroff, Z., Jouravlev, O., and Fedorenko, E. (2022). An investigation across 45 languages and 12 language families reveals a universal language network. *Nature Neuroscience*, 25(8):1014–1019.
- Manning, L. and Thomas-Antérion, C. (2011). Marc Dax and the discovery of the lateralisation of language in the left cerebral hemisphere. *Revue Neurologique*, 167(12):868–872.
- Matchin, W. and Hickok, G. (2020). The Cortical Organization of Syntax. *Cerebral Cortex*, 30(3):1481–1498.
- McKinney, W. et al. (2010). Data structures for statistical computing in python. In *Proceedings of the 9th Python in Science Conference*, volume 445, pages 51–56. Austin, TX.
- Merity, S., Xiong, C., Bradbury, J., and Socher, R. (2016). Pointer sentinel mixture models. *arXiv preprint arXiv:1609.07843*.

- Olulade, O. A., Seydell-Greenwald, A., Chambers, C. E., Turkeltaub, P. E., Dromerick, A. W., Berl, M. M., Gaillard, W. D., and Newport, E. L. (2020). The neural basis of language development: Changes in lateralization over age. *Proceedings of the National Academy of Sciences*, 117(38):23477–23483.
- Ozernov-Palchik, O., O’Brien, A. M., Lee, E. J., Richardson, H., Romeo, R., Lipkin, B., Small, H., Capella, J., Nieto-Castanon, A., Saxe, R., Gabrieli, J. D. E., and Fedorenko, E. (2024). Precision fMRI reveals that the language network exhibits adult-like left-hemispheric lateralization by 4 years of age.
- Pallier, C., Devauchelle, A.-D., and Dehaene, S. (2011). Cortical representation of the constituent structure of sentences. *Proceedings of the National Academy of Sciences*, 108(6):2522–2527.
- Pasquiou, A., Lakretz, Y., Hale, J., Thirion, B., and Pallier, C. (2022). Neural language models are not born equal to fit brain data, but training helps. *arXiv preprint arXiv:2207.03380*.
- Pasquiou, A., Lakretz, Y., Thirion, B., and Pallier, C. (2023). Information-Restricted Neural Language Models Reveal Different Brain Regions’ Sensitivity to Semantics, Syntax, and Context. *Neurobiology of Language*, 4(4):611–636.
- Paszke, A., Gross, S., Massa, F., Lerer, A., Bradbury, J., Chanan, G., Killeen, T., Lin, Z., Gimelshein, N., Antiga, L., et al. (2019). Pytorch: An imperative style, high-performance deep learning library. *Advances in neural information processing systems*, 32.
- Patterson, K. and Lambon Ralph, M. A. (2016). The Hub-and-Spoke Hypothesis of Semantic Memory. In *Neurobiology of Language*, pages 765–775. Elsevier.
- Pedregosa, F., Varoquaux, G., Gramfort, A., Michel, V., Thirion, B., Grisel, O., Blondel, M., Prettenhofer, P., Weiss, R., Dubourg, V., et al. (2011). Scikit-learn: Machine learning in Python. *Journal of machine learning research*, 12(Oct):2825–2830.
- Penfield, W. and Roberts, L. (1959). *Speech and Brain Mechanisms*. Princeton University Press, Princeton, NJ.
- Pennington, J., Socher, R., and Manning, C. D. (2014). Glove: Global vectors for word representation. In *Proceedings of the 2014 conference on empirical methods in natural language processing (EMNLP)*, pages 1532–1543.
- Pobric, G., Jefferies, E., and Lambon Ralph, M. A. (2010). Amodal semantic representations depend on both anterior temporal lobes: Evidence from repetitive transcranial magnetic stimulation. *Neuropsychologia*, 48(5):1336–1342.
- Poizner, H., Bellugi, U., and Klima, E. (1987). *What the Hand reveals about the Brain*. MIT Press, Cambridge, MA.
- Poldrack, R. A. (2011). Inferring mental states from neuroimaging data: From reverse inference to large-scale decoding. *Neuron*, 72(5):692–697.
- Price, A. R., Bonner, M. F., Peelle, J. E., and Grossman, M. (2015). Converging evidence for the neuroanatomic basis of combinatorial semantics in the angular gyrus. *Journal of Neuroscience*, 35(7):3276–3284.
- Pylkkänen, L. (2019). The neural basis of combinatorial syntax and semantics. *Science*, 366(6461):62–66.
- Radford, A., Wu, J., Child, R., Luan, D., Amodei, D., Sutskever, I., et al. (2019). Language models are unsupervised multitask learners. *OpenAI blog*, 1(8):9.
- Schrimpf, M., Blank, I. A., Tuckute, G., Kauf, C., Hosseini, E. A., Kanwisher, N., Tenenbaum, J. B., and Fedorenko, E. (2021). The neural architecture of language: Integrative modeling converges on predictive processing. *Proceedings of the National Academy of Sciences*, 118(45).

- Schrimpf, M., Kubilius, J., Hong, H., Majaj, N. J., Rajalingham, R., Issa, E. B., Kar, K., Bashivan, P., Prescott-Roy, J., Geiger, F., et al. (2020). Brain-score: Which artificial neural network for object recognition is most brain-like? *BioRxiv*, page 407007.
- Seabold, S. and Perktold, J. (2010). statsmodels: Econometric and statistical modeling with python. In *9th Python in Science Conference*.
- Seghier, M. L., Fagan, E., and Price, C. J. (2010). Functional subdivisions in the left angular gyrus where the semantic system meets and diverges from the default network. *The Journal of Neuroscience: The Official Journal of the Society for Neuroscience*, 30(50):16809–16817.
- Simony, E., Honey, C. J., Chen, J., Lositsky, O., Yeshurun, Y., Wiesel, A., and Hasson, U. (2016). Dynamic reconfiguration of the default mode network during narrative comprehension. *Nature Communications*, 7(1):12141. Number: 1 Publisher: Nature Publishing Group.
- Snowden, J. S., Harris, J. M., Thompson, J. C., Kobylecki, C., Jones, M., Richardson, A. M., and Neary, D. (2018). Semantic dementia and the left and right temporal lobes. *Cortex*, 107:188–203.
- Stromswold, K., Caplan, D., Alpert, N., and Rauch, S. (1996). Localization of syntactic comprehension by positron emission tomography. *Brain and language*, 52(3):452–473.
- Szaflarski, J. P., Holland, S. K., Schmithorst, V. J., and Byars, A. W. (2006). fMRI study of language lateralization in children and adults. *Human brain mapping*, 27(3):202–212.
- Team, G., Mesnard, T., Hardin, C., Dadashi, R., Bhupatiraju, S., Pathak, S., Sifre, L., Rivière, M., Kale, M. S., Love, J., et al. (2024). Gemma: Open models based on gemini research and technology. *arXiv preprint arXiv:2403.08295*.
- Toneva, M. and Wehbe, L. (2019). Interpreting and improving natural-language processing (in machines) with natural language-processing (in the brain). *Advances in neural information processing systems*, 32.
- Touvron, H., Martin, L., Stone, K., Albert, P., Almahairi, A., Babaei, Y., Bashlykov, N., Batra, S., Bhargava, P., Bhosale, S., et al. (2023). Llama 2: Open foundation and fine-tuned chat models. *arXiv preprint arXiv:2307.09288*.
- Tzourio-Mazoyer, N., Perrone-Bertolotti, M., Jobard, G., Mazoyer, B., and Baci, M. (2017). Multi-factorial modulation of hemispheric specialization and plasticity for language in healthy and pathological conditions: A review. *Cortex*, 86:314–339.
- Van Der Walt, S., Colbert, S. C., and Varoquaux, G. (2011). The numpy array: a structure for efficient numerical computation. *Computing in Science & Engineering*, 13(2):22.
- Vaswani, A., Shazeer, N., Parmar, N., Uszkoreit, J., Jones, L., Gomez, A. N., Kaiser, Ł., and Polosukhin, I. (2017). Attention is all you need. *Advances in neural information processing systems*, 30.
- Vigneau, M., Beaucousin, V., Hervé, P.-Y., Jobard, G., Petit, L., Crivello, F., Mellet, E., Zago, L., Mazoyer, B., and Tzourio-Mazoyer, N. (2011). What is right-hemisphere contribution to phonological, lexico-semantic, and sentence processing? *NeuroImage*, 54(1):577–593.
- Wada, J. and Rasmussen, T. (1960). Intracarotid Injection of Sodium Amytal for the Lateralization of Cerebral Speech Dominance: Experimental and Clinical Observations. *Journal of Neurosurgery*, 17(2):266–282. Publisher: Journal of Neurosurgery Publishing Group Section: Journal of Neurosurgery.
- Waskom, M. L. (2021). seaborn: statistical data visualization. *Journal of Open Source Software*, 6(60):3021.
- Wernicke, C. (1874). *Der aphasische Symptomencomplex: eine psychologische Studie auf anatomischer Basis*. Cohn & Weigert.

- Wildgruber, D., Ackermann, H., Kreifelts, B., and Ethofer, T. (2006). Cerebral processing of linguistic and emotional prosody: fMRI studies. *Progress in brain research*, 156:249–268. Publisher: Elsevier.
- Witelson, S. F. and Pallie, W. (1973). Left hemisphere specialization for language in the newborn: Neuroanatomical evidence of asymmetry. *Brain*, 96(3):641–646.
- Wolf, T., Debut, L., Sanh, V., Chaumond, J., Delangue, C., Moi, A., Cistac, P., Rault, T., Louf, R., Funtowicz, M., et al. (2020). Transformers: State-of-the-art natural language processing. In *Proceedings of the 2020 conference on empirical methods in natural language processing: system demonstrations*, pages 38–45.
- Wood, A. G., Harvey, A. S., Wellard, R. M., Abbott, D., Anderson, V., Kean, M., Saling, M., and Jackson, G. D. (2004). Language cortex activation in normal children. *Neurology*, 63(6):1035–1044.
- Xu, J., Kemeny, S., Park, G., Frattali, C., and Braun, A. (2005). Language in context: emergent features of word, sentence, and narrative comprehension. *NeuroImage*, 25(3):1002–1015.
- Zaccarella, E. and Friederici, A. D. (2016). The neurobiological nature of syntactic hierarchies. *Neuroscience & Biobehavioral Reviews*.
- Zaccarella, E., Schell, M., and Friederici, A. D. (2017). Reviewing the functional basis of the syntactic Merge mechanism for language: A coordinate-based activation likelihood estimation meta-analysis. *Neuroscience & Biobehavioral Reviews*, 80:646–656.
- Zellers, R., Holtzman, A., Bisk, Y., Farhadi, A., and Choi, Y. (2019). Hellaswag: Can a machine really finish your sentence? *arXiv preprint arXiv:1905.07830*.
- Zhang, S., Roller, S., Goyal, N., Artetxe, M., Chen, M., Chen, S., Dewan, C., Diab, M., Li, X., Lin, X. V., et al. (2022). Opt: Open pre-trained transformer language models. *arXiv preprint arXiv:2205.01068*.

## A Supplementary Tables

Table A.1: List of all 28 large language models included in the study, grouped by family.

model name	$n_{\text{parameters}}$	$n_{\text{layers}}$	$n_{\text{neurons}}$
gpt2	124M	12	768
gpt2-medium	355M	24	1024
gpt2-large	774M	36	1280
gpt2-xl	1.56B	48	1600
opt-125m	125M	12	768
opt-350m	331M	24	1024
opt-1.3b	1.32B	24	2048
opt-2.7b	2.65B	32	2560
opt-6.7b	6.66B	32	4096
opt-13b	1.29B	40	5120
Llama-2-7b-hf	6.74B	32	4096
Llama-2-13b-hf	13.02B	40	5120
Qwen1.5-0.5B	464M	24	1024
Qwen1.5-1.8B	1.84B	24	2048
Qwen1.5-4B	3.95B	40	2560
Qwen1.5-7B	7.72B	32	4096
Qwen1.5-14B	14.17B	40	5120
gemma-2b	2.51B	18	2048
gemma-7b	8.54B	28	3072
stablelm-2-1_6b	1.64B	24	2048
stablelm-3b-4e1t	2.80B	32	2560
stablelm-2-12b	12.14B	40	5120
Mistral-7B-v0.1	7.24B	32	4096
mamba-130m-hf	129M	24	768
mamba-370m-hf	372M	48	1024
mamba-790m-hf	793M	48	1536
mamba-1.4b-hf	1.37B	48	2048
mamba-2.8b-hf	2.77B	64	2560

Table A.2: **Per ROI tests of the interaction between hemisphere and model size.** The first column is the name of each ROI. The second column gives the p-value of the two sample t-test between the set of slopes of all the voxels of the left vs. the right corresponding ROI, whose means and 95% confidence intervals are depicted in Fig. 7b. The third column presents the correlation between the difference in performance of the models (the  $r$ -scores) on the left hemisphere minus the right hemisphere as a function of the logarithm of the number of parameters, as described in Fig. 7c. The last column gives the p-value of the correlation. These two measures of interaction lead to the same conclusions: the interaction is not significant for BA44 and TP (marginal in the latter case), and highly significant for all the other ROIs, namely aSTS, pSTS, AG\_TPJ, BA45 and BA47.

ROI	p-value of two sample t-test	correlation L-R vs. $\log(n_{\text{parameters}})$	p-value
TP	7.1e-02	0.32	9.5e-02
aSTS	5.2e-10	0.84	3.1e-08
pSTS	7.3e-09	0.81	2.0e-07
AG_TPJ	2.5e-20	0.85	1.3e-08
BA44	5.3e-01	0.13	5.2e-01
BA45	9.3e-07	0.73	1.1e-05
BA47	1.1e-04	0.52	4.1e-03

## B Supplementary Figures

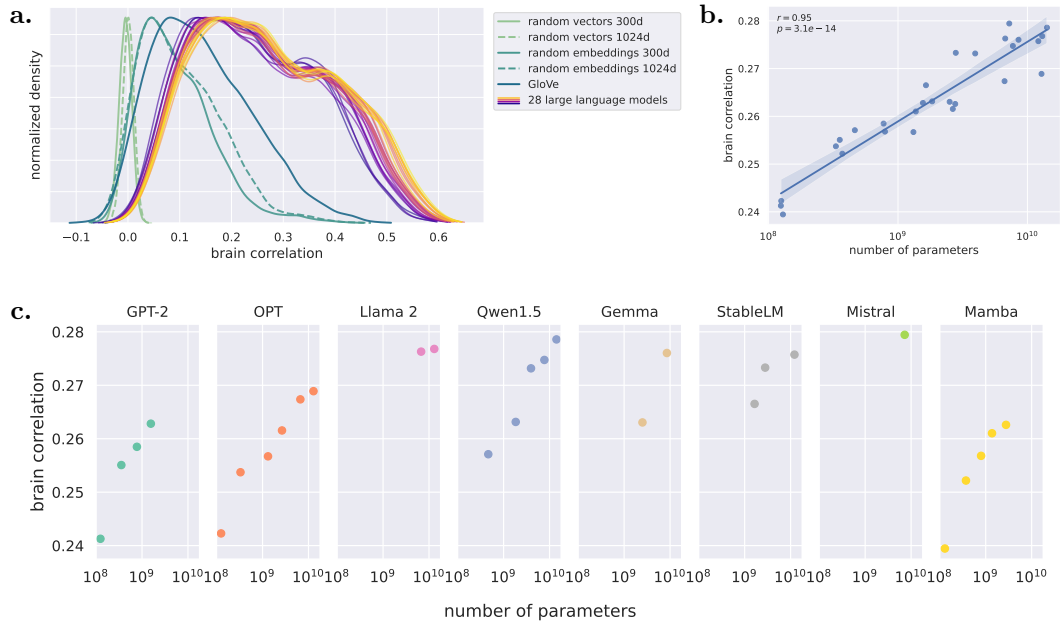


Figure B.1: **Performance of various models in predicting fMRI brain time-courses.** Same as Fig. 2, but for the whole brain volume.

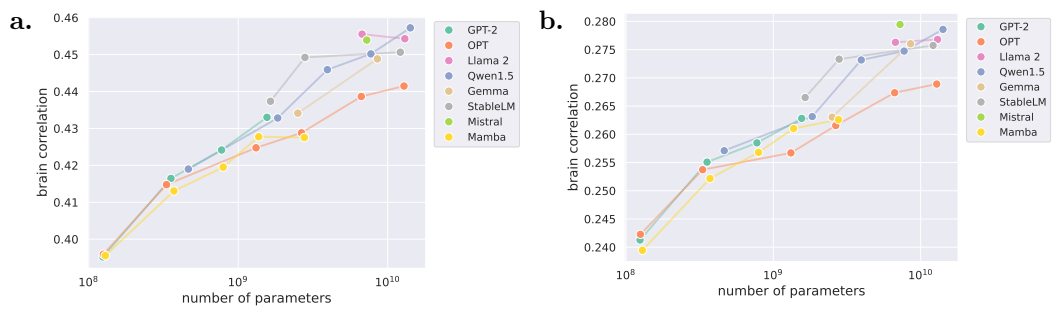


Figure B.2: **Scaling law of fMRI encoding models, by family.** (a) Average over the 25% most reliable voxels (b) Average over the whole brain volume.

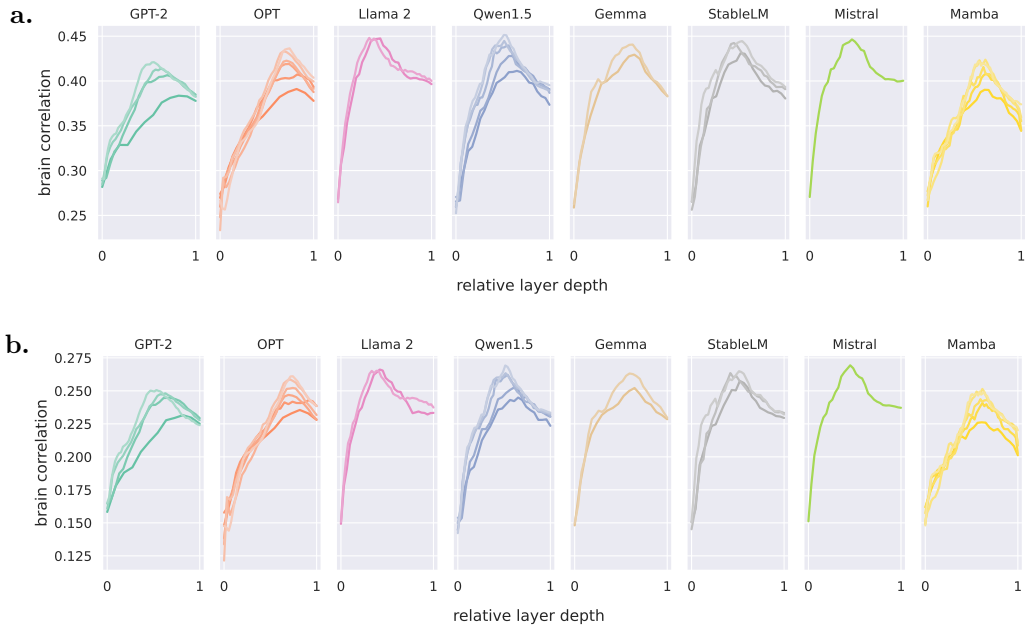


Figure B.3: **Brain correlation as a function of the relative layer depth, split by family.** The relative layer depth corresponds to the depth of a given layer relative to the input and output layers: the first layer is the non-contextual embedding layer, at position 0, and the last hidden layer is at position 1. Considering (a) the 25% most reliable voxels or (b) the whole brain volume.

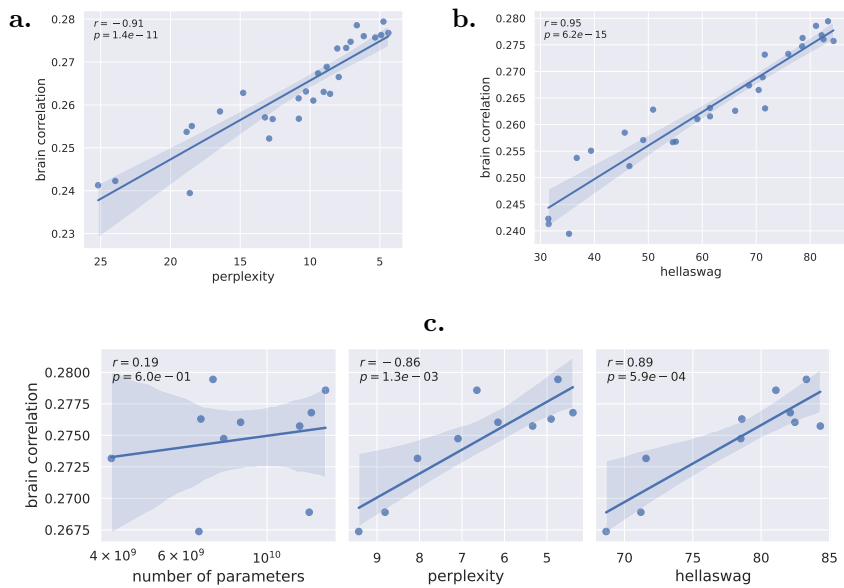


Figure B.4: **Brain correlation and performance on natural language tasks.** Same as Fig. 5, but for the whole brain volume.

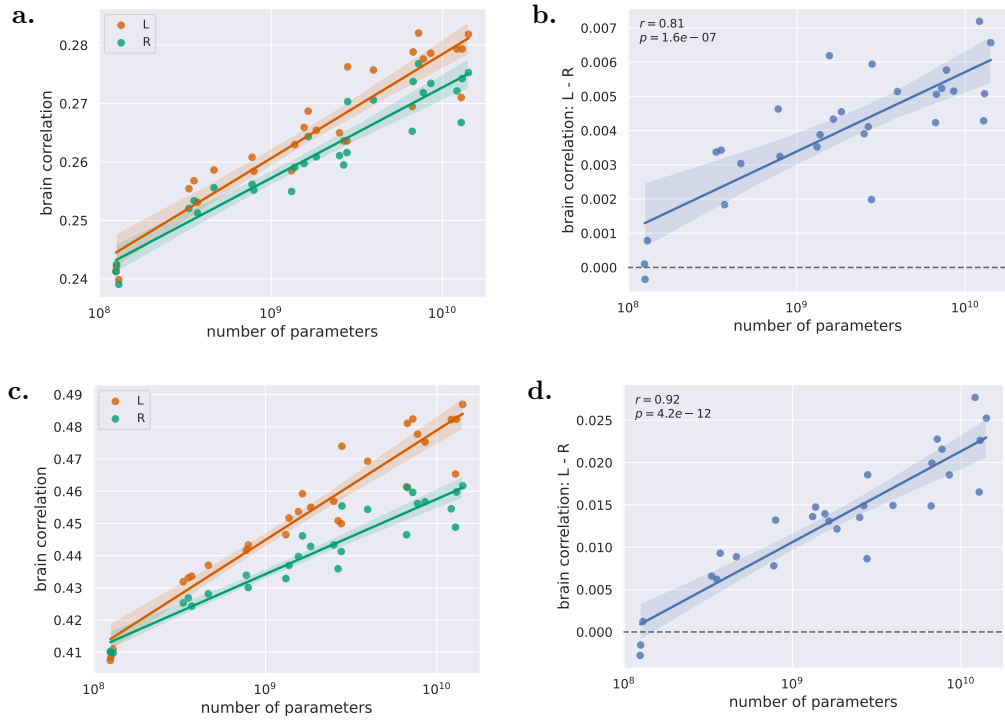


Figure B.5: **Emergence of left lateralization with the size of the encoding models.** Same as Fig. 6, but, top panels (a) and (b), for the whole brain volume, and bottom panels (c) and (d) considering the best 10% voxels of the left hemisphere vs. the best 10% voxels of the right hemisphere.

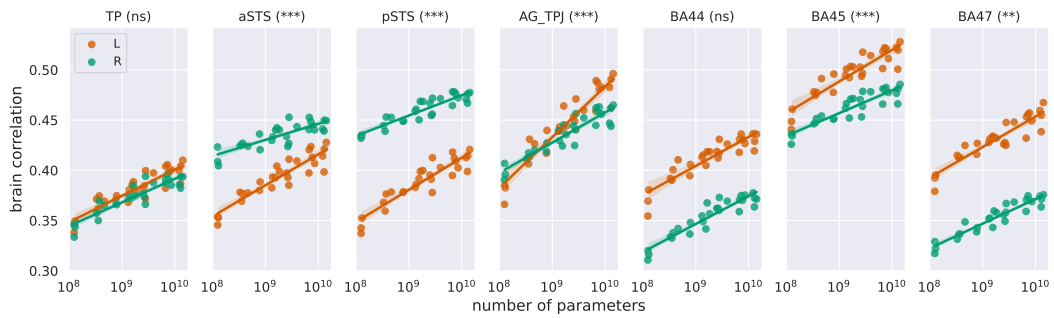


Figure B.6: **Analysis by Regions of Interest.** Brain correlation as a function of the logarithm of the number of parameters, for all 28 models, for each ROI.